



Article

Diurnal Evolution of the Wintertime Boundary Layer in Urban Beijing, China: Insights from Doppler Lidar and a 325-m Meteorological Tower

Yuanjian Yang¹, Sihui Fan^{1,2}, Linlin Wang^{1,2,*}, Zhiqiu Gao^{1,2}, Yuanjie Zhang¹, Han Zou², Shiguang Miao³, Yubin Li¹, Meng Huang¹, Steve Hung Lam Yim^{4,5,6} and Simone Lolli^{7,8}

¹ Collaborative Innovation Centre on Forecast and Evaluation of Meteorological Disasters, School of Atmospheric Physics, Nanjing University of Information Science & Technology, Nanjing 210044, China; yyj1985@nuist.edu.cn (Y.Y.); sihuif_1017@nuist.edu.cn (S.F.); zgao@mail.iap.ac.cn (Z.G.); yuanjiez@nuist.edu.cn (Y.Z.); liyubin@nuist.edu.cn (Y.L.); mhuang@nuist.edu.cn (M.H.)

² State Key Laboratory of Atmospheric Boundary Layer Physics and Atmospheric Chemistry (LAPC), Institute of Atmospheric Physics, Chinese Academy of Sciences, Beijing 100029, China; zouhan@mail.iap.ac.cn

³ Institute of Urban Meteorology, China Meteorological Administration, Beijing 100081, China; sgmiao@ium.cn

⁴ Department of Geography and Resource Management, The Chinese University of Hong Kong, Hong Kong, China; steveyim@cuhk.edu.hk

⁵ Institute of Environment, Energy and Sustainability, The Chinese University of Hong Kong, Hong Kong, China

⁶ Stanley Ho Big Data Decision Analytics Research Centre, The Chinese University of Hong Kong, Hong Kong, China

⁷ National Research Council, Institute of Methodologies for Environmental Analysis, 85050 Tito (PZ), Italy; simone.lolli@imaa.cnr.it

⁸ Department of Physics, Kent State University (Florence Campus), Kent, OH 44240, USA

* Correspondence: linlinwang@mail.iap.ac.cn

Received: 21 October 2020; Accepted: 27 November 2020; Published: 1 December 2020



Abstract: The diurnal evolution of the atmospheric boundary layer—the lowermost part of the atmosphere where the majority of human activity and meteorological phenomena take place—is described by its depth. Additionally, the boundary layer height (BLH) and the turbulence intensity strongly impact the pollutant diffusion, especially during transition periods. Based on integrated observations from a 325-m meteorological tower and a Doppler Wind lidar in the center of Beijing, the entire diurnal cycle of urban BLH in December 2016 was characterized. Results highlight that the Doppler lidar exhibited it is well suited for monitoring convective BLH while it trudges in monitoring stable BLH, while a 325-m meteorological tower provided an important supplement for Doppler lidar under nocturnal boundary layer and heavily polluted conditions. For the diurnal cycle, under light wind condition, the pattern of urban BLH was largely modulated by thermal forcing of solar radiation and may partly be affected by wind speed. While under strong wind condition, the pattern of urban BLH was largely modulated both by thermal forcing and dynamical forcing. The present work also presented evidence for several new features in the morning and afternoon transitions of the urban boundary layer, showing the duration of the morning transition varied between 1 and 5 h, with the largest value occurring under weak wind with high PM_{2.5} concentration; while the afternoon transition ranged from 3 to 6 h, which was positively (negatively) correlated to wind speed (PM_{2.5} concentration). Our work highlights that weak wind speed (weak dynamic motion) and heavy aerosol pollution (weak thermal forcing due to the effect of cooling) can dramatically affect the evolution of the boundary layer.

Keywords: boundary layer height; urban boundary layer; Doppler wind lidar; 325-m meteorological tower

1. Introduction

The atmospheric boundary layer (ABL) height is an important factor in diluting pollutants emitted at the surface, in which layered pollutants vertically disperse through the action of turbulence. Accurate estimation of ABL diurnal variability is critical to predict pollutant concentrations by model computations [1–4], especially for the ABL over urban environment, so-called the urban boundary layer [5–7]. The most common way to determine the boundary layer height (BLH) is by using vertical profiles of meteorological variables, such as the potential temperature, wind speed (WS), and bulk Richardson number (Ri_b), which are generally obtained from radiosonde launches or aircraft observations [8]. However, radiosonde observations are usually infrequent and rarely made in central urban environments [9]. Mostly, radio soundings collected at rural sites nearby cities are used to assist in the analysis of the urban boundary layer [10,11]. Particularly, spatial differences in daytime BLH have been reported due to various surface properties with different surface heat flux characteristics [12,13]. Thus, the BLH estimated from radio soundings launched at rural sites is not representative of urban areas. Moreover, in the frame of the World Meteorological Organization (WMO), the radio soundings are launched only twice per day. In few other locations, i.e., during field campaigns and densified observation, radio-sounding are launched three times a day and therefore cannot capture the diurnal development of the urban boundary layer.

In the last decades, remote sensing techniques and network of instruments became the most valuable and popular approach for detecting the nature of the atmosphere [14], particularly in the urban layer, because of their higher temporal resolutions, such as ceilometers [15,16], sodars [17,18], and lidars [1,11]. The Doppler wind lidar is an optical active remote sensing instrument that became popular after the discovery of the CO₂ laser [19,20]. Compared to other lidar types (e.g., elastic and Raman), Doppler wind lidar is the most suited for the investigation of the vertical wind structures, the development of the urban boundary layer [3,19–25], and for validating numerical forecast models [26] as it has the capability to measure the 3D wind vector field with the maximum measurement range exceeding 10 km. For instance, the vertical velocity variance (σ_w^2), obtained from the 3D wind measurements, can be used to describe the turbulence intensity by the turbulence method, and the BLH can be defined. The urban mixing height was defined by using a threshold method (the so-called threshold method) as the height up to which $\sigma_w^2 > 0.1 \text{ m}^2 \text{ s}^{-2}$ in London, UK [21]. A previous study pointed out that the threshold method provides a reliable height retrieval for convective boundary layer (CBL) with strong turbulence and unstable atmospheric stratification but is not recommended to determine the nocturnal boundary layer (NBL) height, when usually the turbulence is weak and often has $\sigma_w^2 < 0.1 \text{ m}^2 \text{ s}^{-2}$ [27]. For another instance, a Doppler wind lidar was set in urban Beijing during the summer of 2015. Our previous study also evaluated a new improved version of the threshold method [28], to determine the NBL height, which defined the NBL top as the height at which σ_w^2 decreases to 10% of its near-surface maximum after subtracting a background value [27]. Based on a case study under heavily polluted conditions (1–4 December 2016), we found that these two threshold methods in London and Beijing were both inaccurate in determining the NBL height [29]. The former was also proven wrong for severely polluted urban boundary layer conditions with weak turbulence during daytime in winter in Beijing. This might have been because of the lower urban BLH dropping below the minimum observable height (100 m) during the time of the NBL. Additionally, the winter NBL over Beijing is mostly steady owing to surface radiative cooling [30,31], which does not satisfy the near-neutral assumption for the method developed by [27]. As is well known, the NBL under fine weather is the most common example of a stable boundary layer (SBL). The NBL often has a complex structure, especially over polluted urban canopies [32], which makes it far more difficult to retrieve the

SBL height by using a solo Doppler lidar. For severely polluted cities, it is therefore necessary to provide measurements of the near-surface layer properties under SBL conditions additional (or auxiliary) to those by Doppler lidar to be able to reliably estimate the diurnal cycle of the BLH.

A tall meteorological tower in Beijing, officially known as “the Beijing 325-m meteorological tower”, is located in the city center, providing 15 levels of measurements of WS and temperature. The main limitation of the tower platform is the observational height. The advantages and disadvantages of the Doppler lidar and tower instruments suggest that urban BLH detection might be improved by using the two instruments in synergy. In this work, by combining the retrievals from the co-located Doppler wind lidar and the 325-m meteorological tower, we aim to estimate the urban BLH and investigate the development of urban BLH in Beijing, especially during heavily polluted conditions, and characterize its full diurnal cycle in winter conditions.

2. Materials and Methods

2.1. Experimental Sites and Instrumentation

The 325-meteorological tower and the Doppler wind lidar (Windcube200, Leosphere, Orsay, France) are co-located at the Institute of Atmospheric Physics (IAP), Chinese Academy Sciences in Beijing city center (39.97°N, 116.37°E) (See Figure 1a).

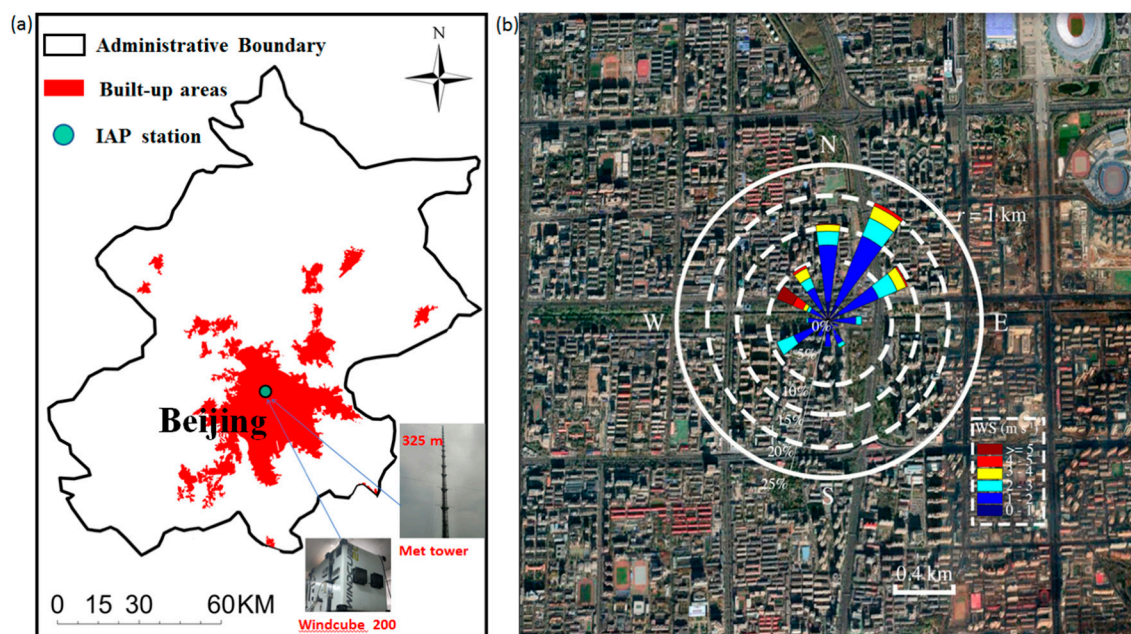


Figure 1. The map of urban Beijing area and location of the 325-meteorological tower and the Doppler wind lidar at the Institute of Atmospheric Physics (IAP) station (a), and the aerial photograph of the urban Beijing area around met tower (4 km × 4 km) (b). The wind rose shows the results observed in these 31 days.

The measurements are taken at 15 levels (i.e., 8 m, 15 m, 32 m, 47 m, 65 m, 80 m, 100 m, 120 m, 140 m, 160 m, 180 m, 200 m, 240 m, 280 m, and 320 m above ground level) by a suite of meteorological instruments (010C cup anemometers, 020C wind vanes, Metone, Grants Pass, OR, USA, HC2-S3, Rotronic, Switzerland) deployed on the 325-m meteorological tower, which provides observations of the WS, wind direction, relative humidity (RH), and air temperature (T) measurements. In addition, turbulence measurements are taken using sonic anemometers (Model Windmaster Pro, Gill, UK) and four-component radiation using downward-pointing and upward-pointing pyrgeometers, and pyranometers (CNR1, Kipp & Zonen, Delft, The Netherlands) are maintained at the same heights (i.e., 47 m, 140 m, and 280 m) on this tower. The detectable range of the lidar spans from 100 m to

several kilometers above the ground (depending on the aerosol concentration), with a vertical range resolution of 50 m.

In addition, the PM_{2.5} mass concentrations measured at the Beijing Olympic Sports Center (Aoti surface station), located approximately 2 km north of IAP station, were obtained from the China National Environmental Monitoring Center website (<http://106.37.208.233:20035/>). Cloud fractions observations were from the Nanjiao weather station, about 20 km from the IAP station.

As shown in Figure 1b, the IAP station is surrounded by a highly dense area of tall buildings. Around this station, there are about 92.1% impervious built-up surfaces and commercial and residential tall buildings (10–60 m), within a radius of 5 km of the tower [33,34]. By using the 47 m level wind measurements, we can speculate that strong northerly winds prevailed in winter, while southerly winds are lighter with a speed lower than 3 m s⁻¹.

2.2. Data Processing

The original 3D sonic anemometer records (10 Hz) were processed prior to analysis using the methods of double rotation (i.e., yaw and pitch rotations) and linear detrending. A density effect correction [35], planar fit method [36], and an averaging period of one hour [37] was applied in the analysis. A criterion of threshold carrier-to-noise ratio of -20 dB [21,27] was chosen to reduce the effects of invalid data in this dataset of the Doppler wind lidar. Based on the edited data, the σ_w^2 over 30-min segments were calculated [21,27].

2.3. Methods

2.3.1. Estimation of Urban BLH

Based on radiosonde data, the Ri_b method is widely used, as it is a reliable method to determine both the CBL and SBL [38]. Compared with the methodology based on detecting the altitude where there is a sharp change in the temperature and RH profiles, the Ri_b method has been found to be more effective, as shown in [39]. The WS and T at 15 levels provided by the 325-m tower make this method available in our study under the condition of BLH < 300 m. The definition of Ri_b was given as [40]:

$$Ri_b(z) = \frac{\frac{g}{\theta_{vs}} (\theta_{vz} - \theta_{vs})(z - z_s)}{(u_z - u_s)^2 + (v_z - v_s)^2 + bu^{*2}} \quad (1)$$

where z is height (m), g is the gravity acceleration constant (m s⁻²), θ_v is the virtual potential temperature (K), u and v are the horizontal components of WS (m s⁻¹), and u^* is the surface friction velocity (m s⁻¹). In addition, z_s is the height of the lower boundary (m), and b is an empirical coefficient. According to [40], z_s can be set to 20 m or 40 m, and b can be set to 100 m. The Ri_b method defines the BLH as the height at which the Ri_b reaches the critical threshold value of 0.25 (the vertical change of Ri_b is shown in Figure S1). It is noted that a strong correlation [correlation coefficient (r), $r = 0.83$] between the BLH derived with $z_s = 20$ m and $z_s = 40$ m. In this paper, we choose $z_s = 20$ m.

In many previous studies, b was set to 0 because of the unknown value of u^* , as in the experiments [41–43]. In our study, u^* can be calculated as $(\overline{u'w'^2} + \overline{v'w'^2})^{1/4}$ by using the sonic anemometer (streamwise u , cross-stream v , and vertical velocities w). As shown in Figure 2, combining the time series of the results with $b = 100$ and $b = 0$ and their one-to-one plot, the sensitivity of the estimation of BLH to the effect of surface friction was studied. Generally, the BLH values computed with $b = 100$ are larger than those with $b = 0$, and the r is just 0.76, which indicates the surface friction effect cannot be ignored. Particularly, the different values in daytime (from sunrise to sunset), in blue, during a red-alert pollution event (17–21 December), reached to about 100 m, with the BLH lower than 150 m for $b = 0$ but larger than 250 m for $b = 100$. This suggests that, in a steadily polluted urban boundary layer with weak buoyancy destruction and shear production during daytime, the surface friction effect plays an important role in the development of the urban boundary layer.

Zhang et al. [44] also found that the surface friction effect had a significant impact on the calculation of BLH, especially for the height of the SBL. Therefore, $b = 100$ was used in our study.

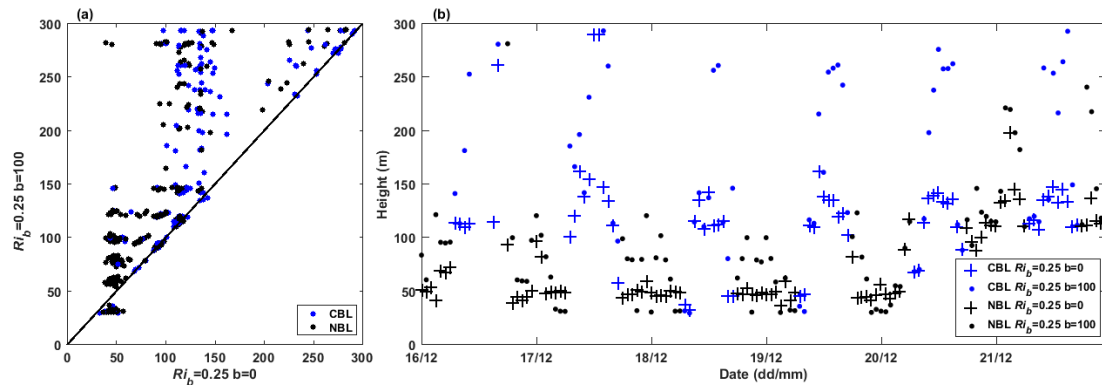


Figure 2. Relationship between the urban boundary layer height (BLH) calculated by using the Ri_b method ($Ri_b = 0.25$) with two different parameter values, $b = 0$ and $b = 100$ for convective boundary layer (CBL) (blue) and nocturnal boundary layer (NBL) (black), during December 2016 (a), and the time series values of BLH values from 16 December to 21 December 2016 (b), $b = 0$ (+) and $b = 100$ (dots).

The standard deviation (σ_w) of the 30-min vertical velocity was calculated by using the measurements from Doppler wind lidar. The threshold method of $\sigma_w^2 > 0.1 \text{ m}^2 \text{ s}^{-2}$ derived by [13], as mentioned in the Introduction, was used to calculate urban BLH based on the lidar.

2.3.2. Calculation of Heat Flux

From the sonic anemometer measurements, the turbulence kinetic energy (TKE) per unit mass of flow (TKE/m, $\text{m}^2 \text{ s}^{-2}$) and sensible heat flux (H , W m^{-2}) were calculated as:

$$\text{TKE/m} = \frac{1}{2}(\overline{u'^2} + \overline{v'^2} + \overline{w'^2}), \quad (2)$$

$$H = \rho C_p \overline{w'T'_v}, \quad (3)$$

where ρ , C_p , and T_v are the air density (kg m^{-3}), the specific heat capacity at a constant pressure ($\text{J kg}^{-1} \text{ K}^{-1}$), and the virtual air temperature (K), respectively.

3. Results

3.1. Urban BLH

The threshold method, based on the lidar data, was not able to yield the NBL height at all times throughout the measurement campaign, because the urban BLH (averaged in one hour) was too low ($< 100 \text{ m}$, not shown). This method was either available for the urban boundary layer retrievals under daytime heavy pollution conditions. Considering as a case study a red-alert pollution event (the air quality index reaches more than 300, which will last for at least three consecutive days) from 16 to 22 December (Figure 3), rarely the threshold method worked in determining the urban BLH during daytime with a small σ_w^2 , especially under heavily polluted conditions (daytime mean concentrations of $\text{PM}_{2.5} > 200 \mu\text{g m}^{-3}$ on 18–21 December). In contrast, the Ri_b method successfully retrieved the NBL height and even the height of the polluted urban boundary layer during daytime, which shows reasonable results by reference to the change in σ_w^2 . Therefore, in our study, the NBL height was estimated by using the Ri_b method. Considering that the blind overlap lidar region was 100 m, the results of urban BLH from threshold method, which was lower than 150 m, were not considered. Note that the two methods are different, while both of them are based on similar physical parameters related to turbulence processes.

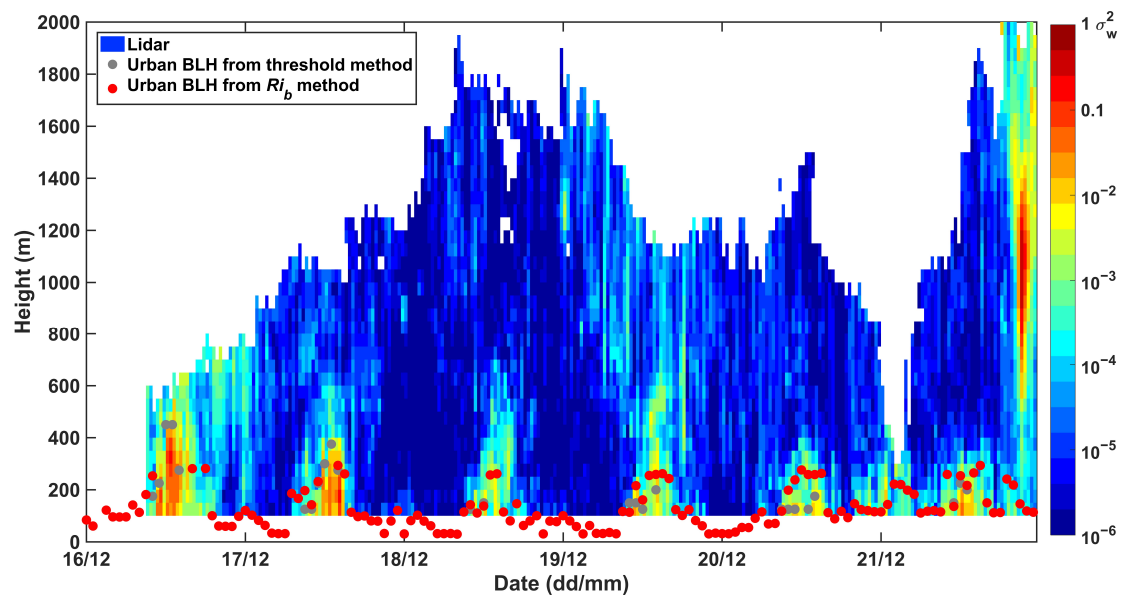


Figure 3. Velocity variance, σ_w^2 ($\text{m}^2 \text{s}^{-2}$), calculated from the Doppler wind lidar data. Derived boundary layer depths, based on the threshold method (grey dots) and Ri_b method (red dots). It should be noted that the blank part of the σ_w^2 can be attributed to a technical failure on 16 December, and the different range spans on different days may mainly depending on the aerosol concentration.

In case that only one method is available to retrieve the boundary layer height, that retrieved value is taken as reference. Instead, when the boundary layer height could be retrieved with the two methods, the intercomparison is shown in Figure 4. Combined with Figure 3, it was found that mostly the boundary layer height retrieved by the Ri_b method is higher with respect to the retrievals obtained with the threshold method, and the urban BLHs from threshold method is rather insensitive for urban BLH below about 200 m. The correlation is essentially nonexistent ($r^2 = 0.16$). Considering that the threshold method may underestimate the depth of mixing layer/the urban boundary layer under weak turbulence context [21,23,27], we use the threshold (200 m) of the definition of the onset of CBL [45] and the height of the meteorology tower (325 m) as the references to choose the different results as the real values. When the height could be retrieved from both the two methods, the urban BLHs retrieved from the Ri_b method was considered as reference (4% of the total values) if the urban BLHs from threshold method were lower than 200 m, and the averaged values were chosen if the urban BLHs from threshold method were larger than or equal to 200 m, and lower than 325 m (3% of the total values) (see Figure 4). About 1% of the urban BLHs retrievals from threshold method were higher than 325 m and also than the values from Ri_b method, which happened during the clean noon time with relatively larger turbulence. Thus, in this condition, the values from threshold method were considered credible and chosen as the real ones.

In addition, through comparison against simulated urban BLH derived by three different BL parameterization schemes (Table S1 in supporting information) in Weather Research and Forecast (WRF) model, it is shown that similar diurnal patterns of urban BLH were captured by our present observation (See Figure S2 in supporting information), implying that the physical process of boundary layer evolution based on our observation is reasonable. While the biases are mainly related to different BLH definitions causing the divergence among different schemes [46]. More details of BLH simulations are available in the study of [46].

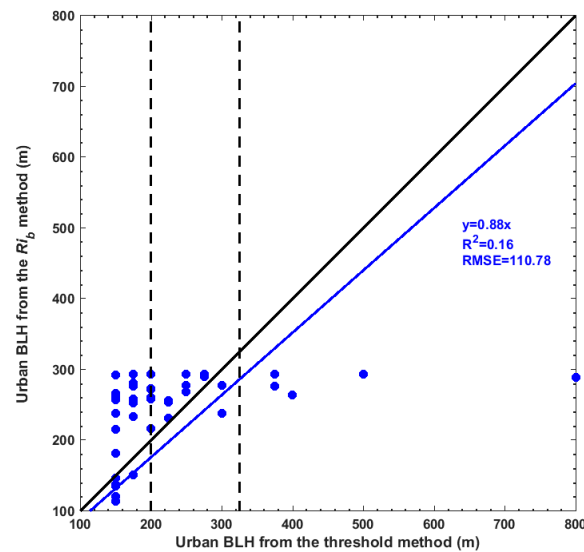


Figure 4. Comparison of the boundary layer depths calculated using Ri_b and threshold methods from 1 to 31 December 2016. Dashed lines: 200 m (definition of the onset of the convective boundary layer) and 325 m (the height of the meteorology tower).

Figure 5 shows the hourly urban BLHs during the whole month (1–31 December), as well as the meteorological conditions [WS, downward shortwave radiation (DSR), H , cloud fraction, and $PM_{2.5}$ concentrations]. Considering that H was found to account for a much larger amount of the net radiation (40%) than the latent heat flux (10%) during this study period over Beijing, only H was shown to represent the heat transfer intensity in this paper. Generally, during this observational period, the urban BLH was positively linked to the near surface WS at all the 15 levels (e.g., $r = 0.3$ and $r = 0.2$ for 8 m and 320 m, respectively), and the largest correlation coefficient, $r = 0.4$, was occurred at 47 m and 65 m, and then decreasing with the increasing height. The Urban BLH was also positively linked to DSR ($r = 0.6$), H ($r = 0.5$), u^* ($r = 0.5$), and TKE/m ($r = 0.5$), but negatively linked to the $PM_{2.5}$ concentrations ($r = -0.4$). A high urban BLH occurred on strong, windy days with a large amount of solar radiation (e.g., 5 December and 23 December). Note that, for very clean windy days with very low aerosols concentration and strong wind as shown in Figure 5b (e.g., 5 December, 8 December, 15 December, and 22 December), the lidar signals showed a low signal-to-noise, resulting in not available data, because the heterodyne Doppler wind lidar technique using an infrared laser source relies on the presence of aerosols [21,27], leading to discontinuous observations as shown in Figure 5a. The maximum urban BLH during the whole winter month was 1000 m, accompanied by the maximum DSR, approximately 480.7 W m^{-2} , on 23 December, which is half that reported on clear days during summer in Beijing by using the threshold method [27]. For a heavily polluted urban boundary layer with weak wind, e.g., 4 December, 18–21 December and 31 December, the maximum urban BLH ranged from 260–300 m, and that of DSR from 240–390 W m^{-2} , during daytime. For the NBL, the heights were mostly around or lower than 200 m, and even lower than 100 m during the heavily polluted conditions.

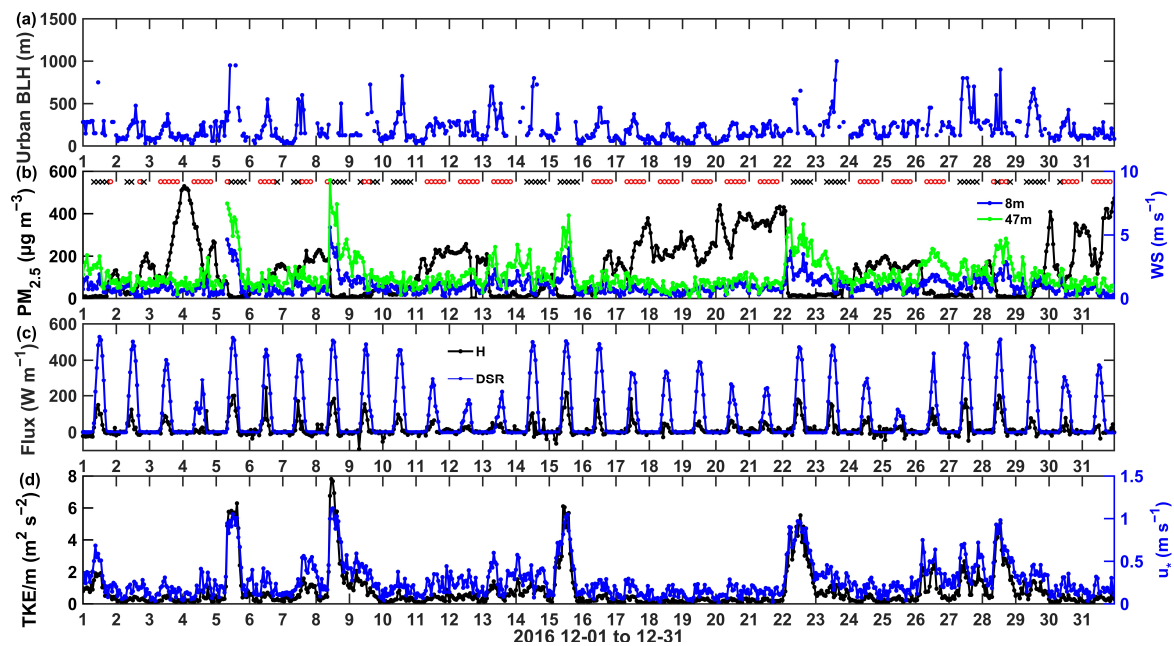


Figure 5. Diurnal cycles of urban BLH derived from threshold method combined with the Richardson number method (a), PM_{2.5} concentration (b), H and DSR (c), and turbulent parameters, TKE and u^* (d). The cloud fraction is marked as red crosses (cloudy) and black crosses (clear).

Based on the retrieved vertical distribution of the aerosol extinction coefficient from a Mie-elastic backscatter polarization lidar (AGHJ-1-LIDAR) developed by Anhui Institute of Optics and Fine Mechanics (AIOFM) also located at the IAP site, the maximum retrieved urban BLH during daytime on 19 and 20 December was 350 m and 300 m in [31], respectively, which is similar to our results (300 m and 278 m). Note, however, that the urban BLH during the early morning was 500 m for these two days but 250 m and 300 m at night in [31], and about 200 m during the early morning on 19 December and 400 m at night on 20 December in [11] by using the same method as [31]. However, urban BLHs were mostly lower than 100 m and exhibited little change during the whole of nighttime (i.e., stable NBL, as shown in Figure S1) in our study. It was found that the stable NBL usually was accompanied by the temperature inversion near the surface during heavily polluted episodes, e.g., during 2–5 December, 16–22 December in [47]. It is important to note that a stable NBL is often coupled with a residual layer (RL) [48]. The aerosol scattering coefficient method probably defines the RL as the stable NBL [49–51]. Thus, attention should be given when comparing aerosol- and turbulence-derived urban BLHs [52], especially when evaluating results from model computations. Nonetheless, the aerosol scattering method provides a useful reference for the RL and NBL, which can help provide an indication of the change of the whole ABL.

To reduce the impact of the diurnal change in meteorological parameters on the urban BLH, the values were averaged for daytime and nighttime. The daily mean urban BLH was in the range of 130–536 m and 64–268 m during daytime and nighttime, with monthly averaged values of 278 m and 152 m, respectively. During the heavily polluted event, the daytime mean urban BLH decreased to <200 m. The lowest BLH during daytime occurred on 18 December, with the lowest WS (0.46 m s^{-1}) at the 8-m level and notably poor turbulent activity ($H = 15.16 \text{ W m}^{-2}$, $u^* = 0.12 \text{ m s}^{-1}$ and $\text{TKE}/\text{m} = 0.11 \text{ m}^2 \text{ s}^{-2}$ at the 47-m level), at which the corresponding daily mean urban BLH during nighttime was only 65 m. The correlation coefficients were calculated between the urban BLH and WS, H and turbulence parameters (u^* and TKE/m), which were 0.6, 0.6, 0.6, and 0.5 during daytime, and 0.6, 0.2, 0.6, and 0.5 at nighttime, respectively. The correlation coefficient between BLH and DSR was 0.6 during daytime. All these above results indicate WS greatly contributed to the change in urban BLH during both daytime and nighttime, because of its direct positive effects on H , u^* and TKE. For instance, on 17

December 2016, weak high-pressure system is to the southeast of Beijing, resulting in southwesterly prevailing weak winds over Beijing (Figure S3). This will induce a weak mixing with lower BLH (Figure 5). In contrast, on 22 December 2016, under the confluence of the high pressure system and the low pressure system (Figure S3), there is a northwest jet in the boundary layer over Beijing, leading to a higher wind speed and strong mixing with higher BLH (Figure 5).

Previous studies demonstrated that pollutant aerosol concentration is directly linked to the urban BLH in Beijing [53,54]. In our study, the correlation coefficient between urban BLH and $PM_{2.5}$ concentration was -0.7 for daytime (at 0.05 significance level) but only -0.5 for nighttime (at 0.05 level significance). This relatively weak correlation for nighttime may have resulted from the small variation range of the BLH during most nights. In addition, as shown in Figure 6, a shallow urban BLH under polluted conditions was usually accompanied by high RH, suggesting that such a humid and shallow BLH favored the accumulation of $PM_{2.5}$. This fact agrees with previous study results in which the generation and transformation of secondary aerosols were found to be significant during humid conditions, leading to an increase of $PM_{2.5}$ concentrations and the resultant occurrence of severe air pollution episodes [55,56]. The daytime urban boundary layer was clean ($PM_{2.5} < 50 \mu g m^{-3}$) once the daily mean urban BLH reached 300 m or above. For nighttime, when the urban BLH was higher than 200 m, the concentration of $PM_{2.5}$ was mostly lower than $100 \mu g m^{-3}$. Meanwhile, it should be noted that for some shallow nighttime urban BLHs (e.g., 9–10 December), defined as urban BLH < 150 m, concentrations of $PM_{2.5}$ were lower than for others, partly explainable by the lower RH, which implies the level of pollution can be attributed to a humid or dry urban boundary layer. Additionally, compared to daytime, aerosol pollutants accumulated more easily in the urban boundary layer at nighttime in Beijing.

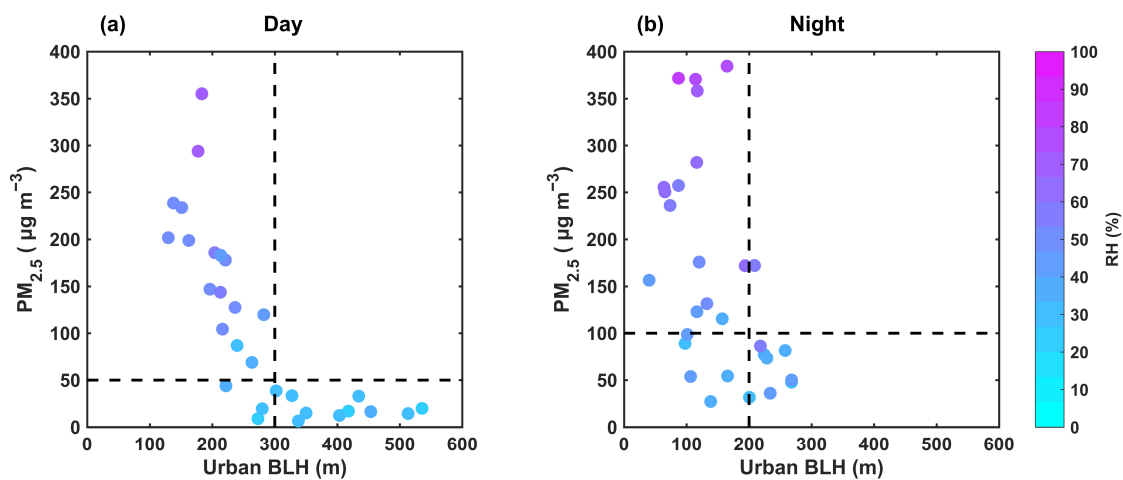


Figure 6. Relationships between $PM_{2.5}$ concentration and urban BLH derived from threshold method combined with the Richardson number method over Beijing during daytime (a) and nighttime (b), with the dots indicating the accompanying RH.

3.2. Diurnal Development of the Urban Boundary Layer

The results presented in the previous section suggest that the near surface WS has a significant effect on urban boundary layer variations in Beijing. Avoiding tall building disturbances around the 325-m tower, the daily average WS measured at the 47-m level was used to classify the different wind conditions. Accordingly, eight, fifteen, and eight days (marked in Figure 7) were categorized as low, medium, and high windy days based on the 25th, 50th, and 75th percentiles of the WS, corresponding to $1.29 m s^{-1}$, $1.54 m s^{-1}$, and $2.23 m s^{-1}$. For low and moderate wind classes, the diurnal changes of WS were not obvious, which indicates the thermal forcing dominates the evolution of the urban boundary layer. Notably, the growth of the boundary layer also influences the wind evolution in boundary layer. Using the measurements at 15 levels from the 325-m tower in 20 years, it was found

that the maximum WS often appeared at daytime at lower levels, while at higher levels the maximum WS usually occurred at nighttime [33], which was resulted from the surface stability of the urban boundary layer. Based on the case study (1–4 December 2016), it was also found that the stagnating urban boundary layer during heavy aerosol polluted daytime in winter seemed to act like an umbrella, preventing the air flow entrainment from the upper level to the lower level [29]. As shown in Figure 7a, different from the strong wind class, the WS showed a downward trend between sunrise and noon for these two wind classes, especially for the weak wind class, which may partly result from the evolution of urban boundary layer.

The diurnal variations of the urban BLH were consistent with those of thermal forcing factors, e.g., solar radiation and sensible heat flux (Figure 7). Especially for weak wind class, with unapparent diurnal change of WS and TKE, the diurnal pattern of urban BLH was mainly modulated by thermal forcing (DSR and H). While under strong wind condition, the diurnal pattern of urban BLH was largely modulated both by dynamical forcing (WS and TKE) and thermal forcing (DSR and H). As shown in Figure 7b1, the DSR decreased with the decreasing wind speed level, which can be attributed to a combination of aerosol pollutants and cloud. These low or moderate wind days were mostly accompanied by high $PM_{2.5}$ concentrations, e.g., $200 \mu\text{g m}^{-3}$ and $100 \mu\text{g m}^{-3}$ median values, as illustrated in Figure 7b3. For the polluted days, particularly the heavily polluted low-wind days, they were usually covered with cloud, as shown in Figure 3, according to the cloud fraction data. However, it is hard to acquire accurate cloud information during heavily polluted periods. In addition, the existing clouds could be the result of polluted aerosols acting as nuclei for cloud formation, during heavy polluted days, more clouds were indeed found over Beijing in case studies [57]. Here, we considered the effects of both aerosol pollutants and cloud on the DSR. On this basis, reduced DSR and weak wind led to weak thermal and dynamic forcing, resulting in a smaller diurnal range of the urban boundary layer on low-wind days than on high-wind days. In other words, compared to strong wind classes as shown in Figure 7f1–f3, a reduction of approximately 400 m and 500 m to the maximum (median values) of the urban BLH for low and moderate classes, respectively, resulted from the combined changes in the wind, the aerosol pollutant concentration, and the cloud fraction. Therefore, it was considerably challenging to quantitatively analyze the radiative feedback effects of aerosol pollutants on the urban boundary layer in Beijing by only using the experimental measurements. As such, model studies should be conducted in the future to help address this issue.

It can also be seen from Figure 7f that the top of the 325-m tower at most times was above the NBL for all the observational period, and the boundary layer during daytime for some cases with low wind in winter, suggesting that the measurements at some of the top levels may have been decoupled from the surface. As mentioned above, the time of CBL onset is defined at the time when the BLH reaches 200 m [39]. Based on this definition, the time of CBL onset got later with weakening wind, and the peak times showed a similar tendency (Figure 7). The growth rate of the median value of urban BLH also differed among the three classes; for example, from 09:00 China Standard Time (CST) to the peak time, the rates were 105 m h^{-1} , 48 m h^{-1} , and 19 m h^{-1} . Moreover, for the strong wind class, some NBL heights were able to reach 200 m in the early morning before sunrise with larger TKE as shown in Figure 7d3, indicating that wind shear production may contribute greatly to the larger BLH during nighttime than for the other wind classes.

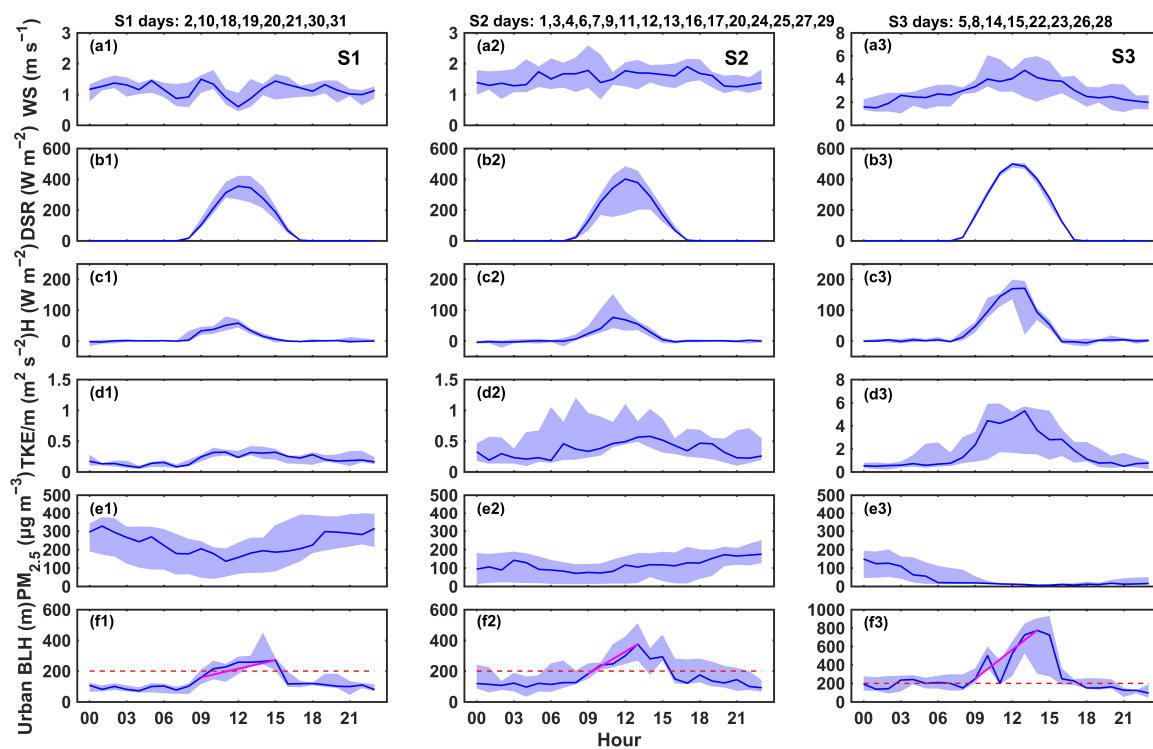


Figure 7. Mean diurnal cycles of downward shortwave radiation (DSR), sensible heat flux, $PM_{2.5}$ concentration, and urban BLH under low (a1,b1,c1,d1,e1,f1), moderate (a2,b2,c2,d2,e2,f2), and strong (a3,b3,c3,d3,e3,f3) wind classes. The shaded areas, blue solid line, red dashed line, and pink lines correspond to the interquartile range (25%–75%), median, 200 m (definition of onset the convective boundary layer), and the slopes of growth rate of the median value of urban BLH from 09:00 CST to the peak time, respectively.

3.3. Morning and Afternoon Transitions of the Urban Boundary Layer

3.3.1. Durations

The CBL starts to grow slowly after sunrise, and a transition feature of both the CBL and SBL, named “morning transition”, is the first stage of the development of the ABL. Examination of the transition periods (e.g., passing from night to day or day to night) has important implications for air quality [58,59]. In previous studies, different algorithms were used to define the morning transition (MT) from observations [57,60,61]. It was defined as the period from the time when the surface buoyancy flux first becomes positive (crossover) to the time at which the BLH reaches about 200 m [57] based on the observations from meteorological tower. Considering the positive heat flux also occurred in nighttime and the urban BLH was often greater than 200 m for urban site during summertime, the beginning of the MT was marked as the sunrise, and the end of MT was defined as the rapid onset of the rapid-growth phase in [58] by using the measurements from a tall tower in London. Given that the positive H occasionally occurred during nighttime in our study period, we defined the sunrise as the starting time of MT. We chose the time when the urban BLH reaches about 200 m as the end of the MT after the sunrise in this wintertime period. The period between the maximum H at midday and $H < 0$ around sunset is usually defined as the afternoon transition (AT) [8,62].

In this paper, we adopted these two methods to estimate the durations of MT and AT during wintertime over horizontally homogeneous Beijing urban surface. Note that the fixed height (200 m) method for MT employed in the present study may not be robust to investigate precise absolute change characteristics of the urban boundary layer. However, at least, it can help us to study the relative change characteristics of the morning development of the urban boundary layer under different conditions

(e.g., wind, solar radiation, pollutants) quantitatively. Similarly, AT is also employed to show relative change characteristics of convective urban boundary layer at daytime.

Excluding strong-wind nights (e.g., 5, 15, and 22 December), the MT duration (D_{MT}) ranged from 1 to 5 h, and the average value was 2.4 h. The maximum D_{MT} occurred on the heavily polluted days, such as 4 and 18 December, with weak morning-averaged winds of 0.6 m s^{-1} and 0.8 m s^{-1} , respectively. The variation of D_{MT} was negatively correlated ($r = -0.4$ for both the 8-m level and 47-m level) with the change in WS, which is consistent with previous studies [57,58,63], and implies that weak wind prolongs the D_{MT} . However, this correlation was weaker than that in [58] ($r = -0.7$), possibly because of the complexity of the aerosol loading. A positive correlation ($r = 0.5$) was found between D_{MT} and $PM_{2.5}$ concentration, which suggests that the significant loading of the aerosol pollutants had large effects on D_{MT} by reducing the net radiation reaching the surface. This can be proved by model results from a large-eddy simulation in which aerosols delayed the CBL onset in the morning by up to 4.5 h [64]. Note that weak wind is usually associated with high concentrations of $PM_{2.5}$ over Beijing; and besides, many other contributing factors, such as stability, advection, the state of the previous day's RL [8], and the entrainment [65], can affect the D_{MT} . The delay in our case was likely caused by a combination of multiple factors.

The AT started at around 11:00–14:00 CST and mostly ended about 1 h before sunset (16:50 CST, monthly averaged), meaning it could last 3–6 h. Interestingly, the AT duration (D_{AT}) showed no obvious correlation with WS ($r < -0.1$), while the ratio of H decay ($r_{\Delta H}$) during D_{AT} showed a strong positive correlation with the WS averaged during D_{AT} ($r = 0.5$ for the 8-m level and $r = 0.6$ for the 47-m level). In addition, $r_{\Delta H}$ had a negative correlation ($r = -0.4$) with the $PM_{2.5}$ concentration averaged during D_{AT} , due to the aerosol cooling effect. In contrast, as compared with a new stable boundary-layer development near the ground in the morning, the boundary layer in the evening was already developed after a growth in the afternoon [66]. This difference will also modulate the magnitude of duration, due to different thermal-dynamical and aerosol context between morning and evening.

Notably, it has been proven that there are interactions between the urban boundary layer and aerosol pollutants [31,67], from which it can be concluded that the long D_{MT} and rapid $r_{\Delta H}$ both support a suitable condition for the accumulation of aerosol pollutants, and in turn, the high concentrations of aerosol pollutants, with their radiation effects, can prolong the D_{MT} and accelerate the $r_{\Delta H}$. Therefore, the transition process is very complex [50], and aerosol pollutants add another level of complexity.

Based on the above findings, a schematic illustration of the diurnal cycle of the ABL on a polluted weak and windy day (taking 19 December as an example) is shown in Figure 8. The RL height (250 m) was taken from [31]. As can be seen, the CBL onset is at 11:00 CST, with a 4-h D_{MT} , which is larger than the mean value (2.4 h). This delayed development is caused by the weak wind (0.7 m s^{-1} at the 8-m level, averaged during D_{MT}) and cooling effect of aerosols ($PM_{2.5}$ concentration = $267 \mu\text{g m}^{-3}$, averaged during D_{MT}). Note that the CBL height tends to decrease obviously from about 4 h after the peak time of H , which implies that the response of the urban BLH variations lag behind the thermal forcing. This result is consistent with previous results derived from observational measurements [8] and a large-eddy model [50]. Moreover, the crossover of H is at 18:00 CST, 1 h after sunset, which can be explained by the weak wind and the high thermal conductivity of the concrete in built-up areas (large heat storage of the urban canopy). The existence of pollutants in the RL, formed on the previous polluted day, plays an important role in the changes of pollutants at the surface in the morning, which can reach the ground the following morning through convection [29,68]. This mechanism of pollutant vertical mixing is very complex, and can be further investigated via model simulations.

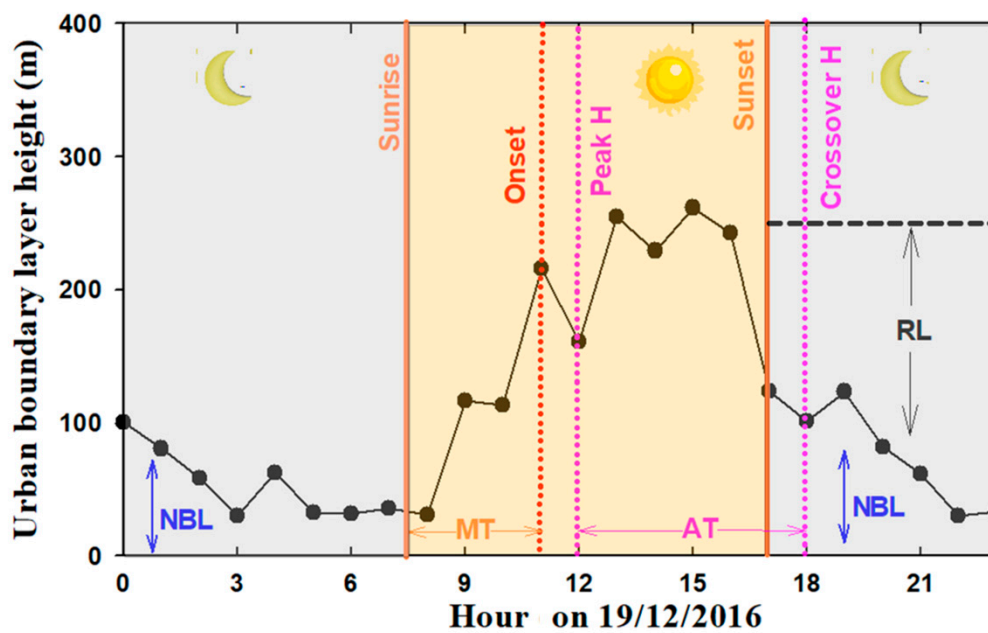


Figure 8. Schematic illustration of the diurnal cycle of the atmospheric boundary layer (ABL) over Beijing on 19 December 2016.

3.3.2. WS and Vertical Variance Profiles

Composite vertical profiles of WS and σ_w^2 averaged in the three wind classes during the MT and AT periods are illustrated in Figure 9. For the median WS profiles, WS was mostly below 5 m s^{-1} and 7 m s^{-1} for weak and moderate wind classes, respectively, while it could reach 17 m s^{-1} at about 1400 m for the strong wind class. Obviously, during MT, low-level jet (LLJ) was detected in all three wind classes, which was mainly attributed to large- and local-scale forcings, e.g., synoptic pattern, local topographic flows, buoyancy, friction, and entrainment processes [69–71]. For the weak wind class, an LLJ occurred at about 400–600 m. Previous studies have revealed that the LLJ can affect the transition of aerosol pollutants via advection flow and vertical mixing [72,73]. A southwesterly LLJ was found in [29], with the jet core at 300–500 m, which might have transferred polluted air from the south via advection to Beijing on 2 December; plus, this LLJ also generated significant wind shear, which could have mixed transported and local pollutants via vertical mixing. In our study, the vertical changes in the wind profile were smaller for weak and moderate wind classes in both the MT and AT periods.

For σ_w^2 , its value was smaller in the MT period than in the AT period (Figure 9), suggesting that the vertical mixing intensity for MT was obviously weaker than for AT for all wind classes. Specifically, the median values of σ_w^2 were $< 0.1 \text{ m}^2 \text{ s}^{-2}$ for MT, while at AT they could reach $0.35 \text{ m}^2 \text{ s}^{-2}$. During the AT period, there was an increasing σ_w^2 between 150 m and 300 m, which can be explained by the strong wind shear as mentioned above. Combined with Figure 7e, it can be clearly seen that weak vertical mixing accompanied high $\text{PM}_{2.5}$ concentrations.

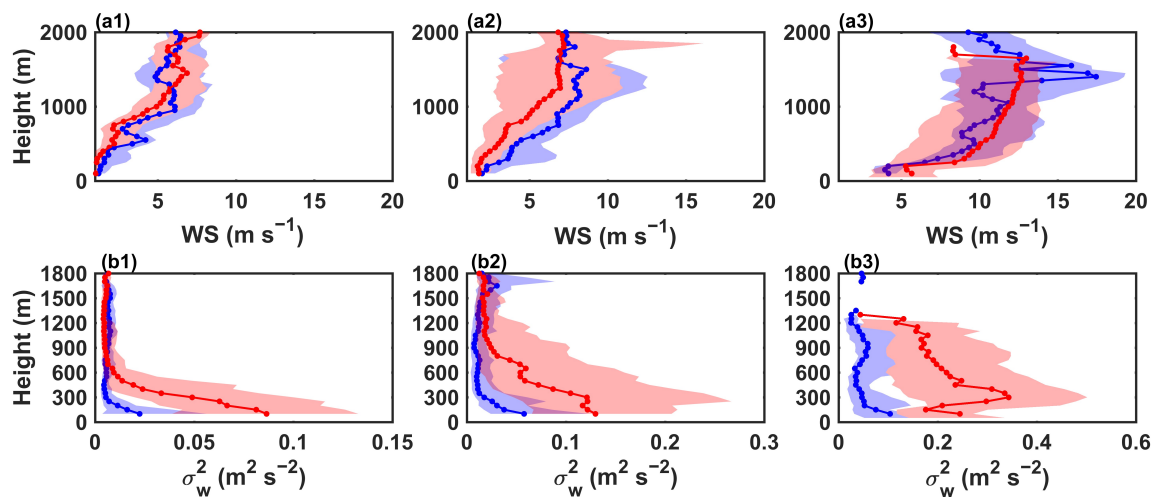


Figure 9. Mean diurnal cycles of WS, (a1,a2,a3) and vertical variance vertical profiles (b1,b2,b3), for weak, moderate, and strong wind classes, respectively. The shaded areas correspond to the interquartile range (25%–75%) during morning (blue) and afternoon transitions (red).

4. Discussions

Note that the aerosol–urban boundary layer interaction is a two-way feedback process [73–75]: (1) the shallow urban boundary layer can weaken the diffusion and dilution condition, accumulating the pollutants, and the resultant aerosol concentration increases at the near-surface. (2) The aerosols can reduce surface solar radiation, suppressing boundary layer development due to the weakened surface heat flux and the weakened thermal forming of underlying surface [34,56,74–77]. In addition, the aerosols in the atmosphere absorbing the shortwave solar radiation could change the vertical temperature stratification (i.e., heating upper air and cooling surface) and further suppress the development of BL [29,75,78]. Such suppressed boundary layer further enhances near-surface aerosol pollution in megacities. In the present study, based on the observational measurements, we mainly focused on the characteristics of the development of the urban boundary layer and concentrations of $\text{PM}_{2.5}$ for different wind classes. Some of these characteristics are resulted from the aerosol–urban boundary layer interaction.

5. Conclusions

In the present study, based on integrated observations from a 325-m meteorological tower and a Doppler lidar in urban Beijing, the entire diurnal cycle of the urban BLH in December 2016 was characterized. The highest daytime urban BLH observed in the measurement campaign was as high as 1000 m; however, under heavily polluted conditions with weak wind, the maximum daytime urban BLH reached up to 300 m only. The Doppler lidar is well suited to retrieve and monitor CBL evolution, while it trudges in monitoring the SBL process. A 325-m meteorological tower provided an important supplement on SBL observation from Doppler lidar, especially under NBL and heavily polluted conditions (urban BLH around or lower than 200 m, and even lower than 100 m). The variations of DSR, WS, H , u^* , and TKE correlated positively with the BLH, while there was a negative correlation between BLH and $\text{PM}_{2.5}$.

Based on the full image of the boundary layer diurnal cycle, we have improved the knowledge of morning and afternoon transitions of the urban boundary layer under different weather and pollution conditions. That is, the D_{MT} varied between 1 and 5 h, with the largest value occurring under conditions of weak wind and high $\text{PM}_{2.5}$ concentration, while D_{AT} ranged from 3 to 6 h. In addition, D_{AT} and $r_{\Delta H}$ presented positive correlations with WS but negative correlations with $\text{PM}_{2.5}$ concentration. Our work highlights that weak WS (weak dynamic motion) and high levels of aerosol pollutants (weak thermal forcing due to the cooling effect) can dramatically affect the development of the boundary layer. For the

diurnal cycle, under weak WS condition, the pattern of urban BLH was largely modulated by thermal forcing of solar radiation and might partly by WS; while for the strong wind condition, the pattern of urban BLH was largely modulated by dynamical forcing (TKE and WS), and as well by thermal forcing.

In future work, many more examples need to be collected to study the impact of thermal and dynamic forcing on the diurnal development of the wintertime boundary layer and its association with air pollution in urban Beijing by using joint meteorological tower and Doppler lidar observations, especially under calm and heavily polluted conditions. The results reported also have important implications for other urban regions that frequently experience air pollution and may aid in designing effective regional mitigation strategies for the environment and human health at the diurnal scale. For instance, according to the different diurnal stages of boundary layer development, we can carry out staggered production strategy to modulate emissions under various urban boundary layer diffusion conditions.

Supplementary Materials: The following are available online at <http://www.mdpi.com/2072-4292/12/23/3935/s1>, Figure S1: Height dependence of Ri_b (calculated by Equation (1) with $b = 100$) at 08:00CST (purple line), 10:00CST (orange line) and 20:00CST (black line) on 19 December, 2016, Figure S2: Hourly variation of simulated PBLH derived by three different PBL parameterization schemes (detail as followings) in Weather Research and Forecast (WRF) model during 16–21, December 2016, Table S1: Properties of the three different boundary layer parameterization schemes.

Author Contributions: Conceptualization, L.W. and Y.Y.; Methodology, S.F., Y.Z. and M.H.; Software, S.F.; Data curation, S.M. and H.Z.; Validation, Z.G., Y.L., S.H.L.Y. and S.L.; Formal analysis, L.W., Y.Y., S.H.L.Y. and S.L.; Writing—original draft preparation Y.Y. and L.W., draft editing S.L. All authors have read and agreed to the published version of the manuscript.

Funding: This work was funded by the National Key Research and Development Program of the Ministry of Science and Technology of China (2016YFC0203304 and 2017YFC0209601).

Acknowledgments: The meteorological elements and heat fluxes measurements from the 325-m tower and the Doppler wind lidar were performed by Institute of Atmospheric Physics, Chinese Academy of science, and the radiation measurements were performed by Institute of Urban Meteorology, China Meteorological Administration. We acknowledge Li Jing at Peking University for supporting the simulation results by using WRF. We also thank Li Aiguo, Jia Jingjing, Tao Yifan and Li Peng for instrument maintenance and data management.

Conflicts of Interest: The authors declare no conflict of interest.

References

1. Collier, C.; Davies, F.; Bozier, K.; Holt, A.; Middleton, D.; Pearson, G.; Siemen, S.; Willetts, D.; Upton, G.; Young, R. Dual Doppler Lidar Measurements for Improving Dispersion Models. *B. Am. Meteorol. Soc.* **2005**, *86*, 825–838. [[CrossRef](#)]
2. White, J.M.; Bowers, J.F.; Hanna, S.R.; Lundquist, J.K. Importance of Using Observations of Mixing Depths in order to Avoid Large Prediction Errors by a Transport and Dispersion Model. *J. Atmos. Ocean. Tech.* **2009**, *26*, 22–32. [[CrossRef](#)]
3. Schween, J.H.; Hirsikko, A.; Löhnert, U.; Crewell, S. Mixing-layer height retrieval with ceilometer and Doppler lidar: From case studies to long-term assessment. *Atmos. Meas. Tech.* **2014**, *7*, 3685–3704. [[CrossRef](#)]
4. Jia, W.X.; Zhang, X.Y. The role of the planetary boundary layer parameterization schemes on the meteorological and aerosol pollution simulations: A review. *Atmos. Res.* **2020**, *239*, 104890. [[CrossRef](#)]
5. Schäfer, K.; Emeis, S.; Hoffmann, H.; Jahn, C. Influence of mixing layer height upon air pollution in urban and sub-urban areas. *Meteorol. Z.* **2006**, *15*, 647–658. [[CrossRef](#)]
6. Salamanca, F.; Martilli, A.; Tewari, M.; Chen, F. A study of the urban boundary layer using different urban parameterizations and high-resolution urban canopy parameters with WRF. *J. Appl. Meteorol. Clim.* **2001**, *50*, 1107–1128. [[CrossRef](#)]
7. Miao, S.G.; Chen, F.; LeMone, M.A.; Tewari, M.; Li, Q.; Wang, Y. An observational and modeling study of characteristics of urban heat island and boundary layer structures in Beijing. *J. Appl. Meteorol. Clim.* **2009**, *48*, 484–501. [[CrossRef](#)]
8. Lothon, M.; Lohou, F.; Pino, D.; Couvreux, F.; Pardyjak, E.R.; Reuder, J.; Vilà-Guerau de Arellano, J.; Durand, P.; Hartogensis, O.; Legain, D.; et al. The BLLAST field experiment: Boundary-Layer Late Afternoon and Sunset Turbulence. *Atmos. Chem. Phys.* **2014**, *14*, 10931–10960. [[CrossRef](#)]

9. Piringer, M.; Joffre, S.; Baklanov, A.; Christen, A.; Deserti, M.; Ridder, K.; Emeis, S.; Mestayer, P.; Tombrou, M.; Middleton, D.; et al. The surface energy balance and the mixing height in urban areas—Activities and recommendations of COST-Action 715. *Boundary-Layer Meteorol.* **2007**, *124*, 3–24. [[CrossRef](#)]
10. Liu, B.M.; Ma, Y.Y.; Gong, W.; Zhang, M.; Yang, J. Determination of boundary layer top on the basis of the characteristics of atmospheric particles. *Atmos. Environ.* **2018**, *178*, 140–147. [[CrossRef](#)]
11. Shi, Y.; Hu, F.; Fan, G.Q.; Zhang, Z. Multiple technical observations of the atmospheric boundary layer structure of a red-alert haze episode in Beijing. *Atmos. Meas. Tech.* **2019**, *12*, 4887–4901. [[CrossRef](#)]
12. Banta, R.M.; Senff, C.J.; White, A.B.; Trainer, M.; McNider, R.T.; Valente, R.J.; Mayor, S.D.; Alvarez, R.J.; Hardesty, R.M.; Parrish, D.; et al. Daytime buildup and nighttime transport of urban ozone in the boundary layer during a stagnation episode. *J. Geophys. Res. Atmos.* **1998**, *103*, 22519–22544. [[CrossRef](#)]
13. Banta, R.M.; White, A.B. Mixing-height differences between land use types: Dependence on wind speed. *J. Geophys. Res. Atmos.* **2003**, *108*, D10. [[CrossRef](#)]
14. Lolli, S.; Paolo, D. Principal component analysis approach to evaluate instrument performances in developing a cost-effective reliable instrument network for atmospheric measurements. *J. Atmos. Ocean.* **2015**, *32*, 1642–1649. [[CrossRef](#)]
15. Kotthaus, S.; Haliou, C.H.; Barlow, J.F.; Grimmond, C.S.B. Volume for pollution dispersion: London’s atmospheric boundary layer during ClearfLo observed with two ground-based lidar types. *Atmos. Environ.* **2018**, *190*, 401–414. [[CrossRef](#)]
16. Yin, J.; Gao, Y.C.; Hong, J.; Gao, Z.Q.; Li, Y.; Li, X.; Zhu, B. Surface meteorological conditions and boundary layer height variations during air pollution episode in Nanjing, China. *J. Geophys. Res. Atmos.* **2018**, *124*, 3350–3364. [[CrossRef](#)]
17. Seibert, P.; Beyrich, F.; Gryning, S.E.; Joffre, S.; Rasmussen, A.; Tercier, P. Review and intercomparison of operational methods for the determination of the mixing height. *Atmos. Environ.* **2000**, *34*, 1001–1027. [[CrossRef](#)]
18. Contini, D.; Cava, D.; Martano, P.; Donato, A.; Grasso, F.M. Comparison of indirect methods for the estimation of boundary layer height over flat-terrain in a coast site. *Meteorol. Z.* **2009**, *18*, 309–320. [[CrossRef](#)]
19. Lolli, S.; Delaval, A.; Loth, C.; Garnier, A.; Flamant, P.H. 0.355-micrometer direct detection wind lidar under testing during a field campaign in consideration of ESA’s ADM-Aeolus mission. *Atmos. Meas. Tech.* **2013**, *6*, 3349–3358. [[CrossRef](#)]
20. Ciofini, M.; Lapucci, A.; Lolli, S. Diffractive optical components for high power laser beam sampling. *J. Opt. A-Pure Appl. Op.* **2003**, *5*, 186–191. [[CrossRef](#)]
21. Barlow, J.F.; Dunbar, T.M.; Nemitz, E.G.; Wood, C.R.; Gallagher, M.W.; Davies, F.; O’Connor, E.; Harrison, R.M. Boundary layer dynamics over London, UK, as observed using Doppler lidar during REPARTEE-II. *Atmos. Chem. Phys.* **2011**, *11*, 2111–2125. [[CrossRef](#)]
22. Park, S.; Kim, S.W.; Park, M.S.; Song, C.K. Measurement of Planetary Boundary Layer Winds with Scanning Doppler Lidar. *Remote Sens.* **2018**, *10*, 1261. [[CrossRef](#)]
23. Yang, Y.J.; Yim, S.H.L.; Haywood, J.; Osborne, M.; Chan, J.C.S.; Zeng, Z.L.; Cheng, J.C.H. Characteristics of Heavy Particulate Matter Pollution Events Over Hong Kong and Their Relationships With Vertical Wind Profiles Using High-Time-Resolution Doppler Lidar Measurements. *J. Geophys. Res. Atmos.* **2019**, *124*, 9609–9623. [[CrossRef](#)]
24. Steve, H.L. Development of a 3D Real-Time Atmospheric Monitoring System (3DREAMS) Using Doppler LiDARs and Applications for Long-Term Analysis and Hot-and-Polluted Episodes. *Remote Sens.* **2020**, *12*, 1036.
25. Huang, T.; Yim, S.-L.; Yang, Y.; Lee, O.-M.; Lam, D.-Y.; Cheng, J.-H.; Guo, J. Observation of Turbulent Mixing Characteristics in the Typical Daytime Cloud-Topped Boundary Layer over Hong Kong in 2019. *Remote Sens.* **2020**, *12*, 1533. [[CrossRef](#)]
26. Liu, Z.L.; Barlow, J.F.; Chan, P.-W.; Fung, J.H.; Li, Y.G.; Ren, C.; Mak, H.W.L.; Ng, E. A Review of Progress and Applications of Pulsed Doppler Wind LiDARs. *Remote Sens.* **2019**, *11*, 2522. [[CrossRef](#)]
27. Huang, M.; Gao, Z.Q.; Miao, S.G.; Chen, F.; LeMone, M.A.; Li, J.; Hu, F.; Wang, L.L. Estimate of boundary-layer depth over Beijing, China, using Doppler Lidar data during SURF-2015. *Boundary-Layer Meteorol.* **2017**, *162*, 503–522. [[CrossRef](#)]

28. LeMone, M.A.; Tewari, M.; Chen, F.; Dudhia, J. Objectively Determined Fair-Weather NBL Features in ARW-WRF and Their Comparison to CASES-97 Observations. *Mon. Weather Rev.* **2014**, *142*, 2709–2732. [[CrossRef](#)]
29. Wang, L.L.; Liu, J.K.; Gao, Z.Q.; Li, Y.B.; Huang, M.; Fan, S.H.; Zhang, X.Y.; Yang, Y.J.; Miao, S.G.; Zou, H.; et al. Vertical observations of the atmospheric boundary layer structure over Beijing urban area during air pollution episodes. *Atmos. Chem. Phys.* **2019**, *19*, 6949–6967.
30. Li, J.; Sun, J.L.; Zhou, M.Y.; Cheng, Z.G.; Li, Q.C.; Cao, X.Y.; Zhang, J.J. Observational analyses of dramatic developments of a severe air pollution event in the Beijing area. *Atmos. Chem. Phys.* **2018**, *18*, 3919–3935. [[CrossRef](#)]
31. Zhong, J.T.; Zhang, X.Y.; Dong, Y.S.; Wang, Y.Q.; Liu, C.; Wang, J.Z.; Zhang, Y.M.; Che, H.C. Feedback effects of boundary-layer meteorological factors on cumulative explosive growth of PM_{2.5} during winter heavy pollution episodes in Beijing from 2013 to 2016. *Atmos. Chem. Phys.* **2018**, *18*, 247–258. [[CrossRef](#)]
32. Pournazeri, S.; Venkatram, A.; Princevac, M.; Tan, S.; Schulte, N. Estimating the height of the nocturnal urban boundary layer for dispersion applications. *Atmos. Environ.* **2012**, *54*, 611–623. [[CrossRef](#)]
33. Liu, J.K.; Gao, Z.Q.; Wang, L.L.; Li, Y.B.; Gao, C.Y. The impact of urbanization on wind speed and surface aerodynamic characteristics in Beijing during 1991–2011. *Meteorol. Atmos. Phys.* **2017**, *130*, 311–324. [[CrossRef](#)]
34. Wang, L.L.; Fan, S.H.; Hu, F.; Miao, S.G.; Yang, A.Q.; Li, Y.B.; Liu, J.J.; Liu, C.W.; Chen, S.S.; Ho, H.C.; et al. Vertical Gradient Variations in Radiation Budget and Heat Fluxes in the Urban Boundary Layer: A Comparison Study Between Polluted and Clean Air Episodes in Beijing During Winter. *J. Geophys. Res. Atmos.* **2020**, *125*, e2020JD032478. [[CrossRef](#)]
35. Detto, M.; Katul, G.G. Simplified expressions for adjusting higher-order turbulent statistics obtained from open path gas analyzers. *Boundary-Layer Meteorol.* **2007**, *122*, 205–216. [[CrossRef](#)]
36. Wilczak, J.M.; Oncley, S.P.; Stage, S.A. Sonic anemometer tilt correction algorithms. *Boundary-Layer Meteorol.* **2001**, *99*, 127–150. [[CrossRef](#)]
37. Wang, L.L.; Li, D.; Gao, Z.Q.; Sun, T.; Guo, X.F.; Bou-Zeid, E. Turbulent transport of momentum and scalars above an urban canopy. *Boundary-Layer Meteorol.* **2014**, *150*, 485–511. [[CrossRef](#)]
38. Seidel, D.J.; Zhang, Y.H.; Beljaars, A.; Golaz, J.-C.; Jacobson, A.R.; Medeiros, B. Climatology of the planetary boundary layer over the continental United States and Europe. *J. Geophys. Res. Atmos.* **2012**, *117*, D17106. [[CrossRef](#)]
39. Wang, D.X.; Stachlewska, I.S.; Song, X.Q.; Heese, B.; Nemuc, A. Variability of the Boundary Layer Over an Urban Continental Site Based on 10 Years of Active Remote Sensing Observations in Warsaw. *Remote Sens.* **2020**, *12*, 340. [[CrossRef](#)]
40. Vogelesang, D.H.P.; Holtlag, A.A.M. Evaluation and model impacts of alternative boundary-layer height formulation. *Boundary Layer Meteorol.* **1996**, *81*, 245–269. [[CrossRef](#)]
41. Zhang, Y.J.; Gao, Z.Q.; Li, D.; Li, Y.B.; Zhang, N.; Zhao, X.; Chen, J. On the computation of planetary boundary-layer height using the bulk Richardson number method. *Geosci. Model Dev.* **2014**, *7*, 2599–2611. [[CrossRef](#)]
42. Guo, J.P.; Miao, Y.C.; Zhang, Y.; Liu, H.; Li, Z.Q.; Zhang, W.C.; He, J.; Lou, M.Y.; Yan, Y.; Bian, L.G.; et al. The climatology of planetary boundary layer height in China derived from radiosonde and reanalysis data. *Atmos. Chem. Phys.* **2016**, *16*, 13309–13319. [[CrossRef](#)]
43. Zhang, Y.H.; Li, S.Y. Climatological characteristics of planetary boundary layer height over Japan. *Int. J. Climatol.* **2019**, *39*, 4015–4028. [[CrossRef](#)]
44. Zhang, Y.J.; Sun, K.; Gao, Z.Q.; Pan, Z.T.; Shook, M.; Li, D. Diurnal climatology of planetary boundary layer height over the contiguous United States derived from AMDAR and reanalysis data. *J. Geophys. Res. Atmos.* **2020**. (under review). [[CrossRef](#)]
45. Angevine, W.M.; Klein, B.H.; Bosveld, F.C. Observations of the morning transition of the convective boundary layer. *Boundary-Layer Meteorol.* **2001**, *101*, 209–227. [[CrossRef](#)]
46. Chu, Y.Q.; Li, J.; Li, C.C.; Tan, W.S.; Su, T.N.; Li, J. Seasonal and diurnal variability of planetary boundary layer height in Beijing: Intercomparison between MPL and WRF results. *Atmos. Res.* **2019**, *227*, 1–23. [[CrossRef](#)]
47. Wang, L.L.; Wang, H.; Liu, J.K.; Gao, Z.Q.; Yang, Y.J.; Zhang, X.Y.; Li, Y.B.; Huang, M. Impacts of the near-surface urban boundary layer structure on PM_{2.5} concentrations in Beijing during winter. *Sci. Total Environ.* **2019**, *669*, 493–504. [[CrossRef](#)]

48. Stull, R.B. *An Introduction to Boundary Layer Meteorology*; Kuwer Academic Publishers: Dordrecht, The Netherlands, 1988; pp. 2–189.
49. Tucker, S.C.; Senff, C.J.; Weickmann, A.M.; Brewer, W.A.; Banta, R.M.; Sandberg, S.P.; Law, D.C.; Hardesty, R.M. Doppler lidar estimation of mixing height using turbulence, shear, and aerosol profiles. *J. Atmos. Ocean. Technol.* **2009**, *26*, 673–688. [[CrossRef](#)]
50. Harvey, N.J.; Hogan, R.J.; Dacre, H.F. A method to diagnose boundary-layer type using Doppler lidar. *Q. J. Roy. Meteor. Soc.* **2013**, *139*, 1681–1693. [[CrossRef](#)]
51. Angevine, W.M.; Edwards, J.M.; Lathon, M.; LeMone, M.A.; Osborne, S.R. Transition Periods in the Diurnally-Varying Atmospheric Boundary Layer Over Land. *Boundary-Layer Meteorol.* **2020**, *53*, 631.
52. Kotthaus, S.; Grimmond, C.S.B. Atmospheric boundary-layer characteristics from ceilometer measurements. Part 1: A new method to track mixed layer height and classify clouds. *Q. J. Roy. Meteor. Soc.* **2018**, *144*, 1525–1538. [[CrossRef](#)]
53. Tang, G.Q.; Zhang, J.Q.; Zhu, X.W.; Song, T.; Munkel, C.; Hu, B.; Schafer, K.; Liu, Z.R.; Zhang, J.K.; Wang, L.L.; et al. Mixing layer height and its implications for air pollution over Beijing, China. *Atmos. Chem. Phys.* **2016**, *16*, 2459–2475. [[CrossRef](#)]
54. Miao, Y.C.; Guo, J.P.; Liu, S.H.; Zhao, C.; Li, X.L.; Zhang, G.; Wei, W.; Ma, Y.J. Impacts of synoptic condition and planetary boundary layer structure on the trans-boundary aerosol transport from Beijing-Tianjin-Hebei region to northeast China. *Atmos. Environ.* **2018**, *181*, 1–11. [[CrossRef](#)]
55. Sun, Y.L.; Jiang, Q.; Wang, Z.F.; Fu, P.Q.; Li, J.; Yang, T.; Yin, Y. Investigation of the sources and evolution processes of severe haze pollution in Beijing in January 2013. *J. Geophys. Res. Atmos.* **2014**, *119*, 4380–4398. [[CrossRef](#)]
56. Li, Z.Q.; Guo, J.P.; Ding, A.J.; Liao, H.; Liu, J.J.; Sun, Y.L.; Wang, T.J.; Xue, H.W.; Zhang, H.S.; Zhu, B. Aerosol and boundary-layer interactions and impact on air quality. *Natl. Sci. Rev.* **2017**, *4*, 810–833. [[CrossRef](#)]
57. Tan, S.C.; Zhang, X.; Wang, H.; Chen, B.; Shi, G.Y.; Shi, C. Comparisons of cloud detection among four satellite sensors on severe haze days in eastern china. *Atmos. Ocean. Sci. Lett.* **2018**, *11*, 86–93. [[CrossRef](#)]
58. Halios, C.H.; Barlow, J.F. Observations of the Morning Development of the Urban Boundary Layer over London, UK, Taken During the ACTUAL Project. *Boundary-Layer Meteorol.* **2018**, *166*, 395–422. [[CrossRef](#)]
59. Price, J. On the formation and development of radiation fog: An observational study. *Boundary-Layer Meteorol.* **2019**, *172*, 167–197. [[CrossRef](#)]
60. Bange, J.; Spiess, T.; van den Kroonenberg, A. Characteristics of the early-morning shallow convective boundary layer from Helipod Flights during STINHO-2. *Theor. Appl. Climatol.* **2007**, *90*, 113–126. [[CrossRef](#)]
61. Pal, S.; Haefelin, M.; Batchvarova, E. Exploring a geophysical process-based attribution technique for the determination of the atmospheric boundary layer depth using aerosol lidar and near-surface meteorological measurements. *J. Geophys. Res. Atmos.* **2013**, *118*, 9277–9295. [[CrossRef](#)]
62. Nadeau, D.F.; Pardyjak, E.; Higgins, C.W.; Fernando, H.J.S.; Parlange, M.B. A simple model for the afternoon and early evening decay of convective turbulence over different land surfaces. *Boundary-Layer Meteorol.* **2011**, *141*, 301–324. [[CrossRef](#)]
63. Beare, R.J. The Role of Shear in the Morning Transition Boundary Layer. *Boundary-Layer Meteorol.* **2008**, *129*, 395–410. [[CrossRef](#)]
64. Barbaro, E.; de Arellano, J.V.-G.; Ouwersloot, H.G.; Schröter, J.S.; Donovan, D.P.; Krol, M.C. Aerosols in the convective boundary layer: Shortwave radiation effects on the coupled land-atmosphere system. *J. Geophys. Res. Atmos.* **2014**, *119*, 5845–5863. [[CrossRef](#)]
65. Driedonks, A.G.M. Models and observations of the growth of the atmospheric boundary layer. *Boundary-Layer Meteorol.* **1982**, *23*, 283–306. [[CrossRef](#)]
66. Donato, A.; Contini, D.; Belosi, F.; Gambaro, A.; Santachiara, G.; Cesari, D.; Prodi, F. Characterisation of PM_{2.5} concentrations and turbulent fluxes on an island of Venice lagoon using high temporal resolution measurements. *Meteorol. Z.* **2012**, *21*, 385–398. [[CrossRef](#)]
67. Zhang, X.Y.; Sun, J.Y.; Wang, Y.Q.; Li, W.J.; Zhang, Q.; Wang, W.G.; Quan, J.N.; Cao, G.L.; Wang, J.Z.; Yang, Y.Q.; et al. Factors contributing to haze and fog in china. *Chin. Sci. Bull.* **2013**, *58*, 1178.
68. Han, S.Q.; Hao, T.Y.; Zhang, Y.F.; Liu, J.L.; Li, P.Y.; Cai, Z.; Zhang, M.; Wang, Q.L.; Zhang, H. Vertical observation and analysis on rapid formation and evolutionary mechanisms of a prolonged haze episode over central-eastern China. *Sci. Total Environ.* **2018**, *616–617*, 135–146. [[CrossRef](#)]

69. Salmond, J.A.; McKendry, I.G. A review of turbulence in the very stable nocturnal boundary layer and its implications for air quality. *Prog. Phys. Geog.* **2015**, *29*, 171–188. [[CrossRef](#)]
70. Miao, Y.C.; Guo, J.P.; Liu, S.H.; Wei, W.; Zhang, G.; Lin, Y.L.; Zhai, P.M. The climatology of low-level jet in Beijing and Guangzhou, China. *J. Geophys. Res. Atmos.* **2018**, *123*, 2816–2830. [[CrossRef](#)]
71. Banta, R.M.; Newsom, R.K.; Lundquist, J.K.; Pichugina, Y.L.; Coulter, R.L.; Mahrt, L. Nocturnal low-level jet characteristics over Kansas during cases-99. *Boundary-Layer Meteorol.* **2002**, *105*, 221–252. [[CrossRef](#)]
72. Hu, X.M.; Ma, Z.Q.; Lin, W.L.; Zhang, H.L.; Hu, J.L.; Wang, Y.; Xu, X.B.; Fuentes, J.D.; Xue, M. Impact of the Loess Plateau on the atmospheric boundary layer structure and air quality in the North China Plain: A case study. *Sci. Total Environ.* **2014**, *499*, 228–237. [[CrossRef](#)]
73. Chen, Y.; An, J.L.; Sun, Y.L.; Wang, X.Q.; Qu, Y.; Zhang, J.W.; Wang, Z.F.; Duan, J. Nocturnal low-level winds and their impacts on particulate matter over the Beijing area. *Adv. Atmos. Sci.* **2018**, *35*, 1455–1468. [[CrossRef](#)]
74. Petäjä, T.; Järvi, L.; Kerminen, V.M.; Ding, A.J.; Sun, J.N.; Nie, W.; Kujansuu, J.; Virkkula, A.; Yang, X.Q.; Fu, C.B.; et al. Enhanced air pollution via aerosol-boundary layer feedback in China. *Sci. Rep.* **2016**, *6*, 1–6. [[CrossRef](#)]
75. Zhong, J.T.; Zhang, X.Y.; Wang, Y.Q.; Wang, J.Z.; Shen, X.J.; Zhang, H.S.; Wang, T.J.; Xie, Z.Q.; Liu, C.; Zhang, H.D.; et al. The two-way feedback mechanism between unfavorable meteorological conditions and cumulative aerosol pollution in various haze regions of China. *Atmos. Chem. Phys.* **2019**, *19*, 3287–3306. [[CrossRef](#)]
76. Yang, Y.J.; Zheng, Z.F.; Yim, S.H.L.; Roth, M.; Ren, G.; Gao, Z.Q.; Wang, T.; Li, Q.; Shi, C.; Ning, G.; et al. PM_{2.5} pollution modulates wintertime Urban-Heat-Island intensity in the Beijing-Tianjin-Hebei megalopolis, China. *Geophys. Res. Lett.* **2020**, *47*, e2019GL084288. [[CrossRef](#)]
77. Ding, A.J.; Fu, C.B.; Yang, X.Q.; Sun, J.N.; Petäjä, T.; Kerminen, V.M.; Wang, T.; Xie, Y.; Herrmann, E.; Zheng, L.F.; et al. Intense atmospheric pollution modifies weather: A case of mixed biomass burning with fossil fuel combustion pollution in eastern China. *Atmos. Chem. Phys.* **2013**, *13*, 10545–10554. [[CrossRef](#)]
78. Lolli, S.; Khor, W.Y.; Matjafri, M.Z.; Lim, H.S. Monsoon season quantitative assessment of biomass burning clear-sky aerosol radiative effect at surface by ground-based lidar observations in Pulau Pinang, Malaysia in 2014. *Remote Sens.* **2019**, *11*, 2660. [[CrossRef](#)]

Publisher’s Note: MDPI stays neutral with regard to jurisdictional claims in published maps and institutional affiliations.



© 2020 by the authors. Licensee MDPI, Basel, Switzerland. This article is an open access article distributed under the terms and conditions of the Creative Commons Attribution (CC BY) license (<http://creativecommons.org/licenses/by/4.0/>).